Biosensors and Bioelectronics 69 (2015) 128–134

Contents lists available at ScienceDirect

Biosensors and Bioelectronics

journal homepage: www.elsevier.com/locate/bios

Silver nanoprism etching-based plasmonic ELISA for the high sensitive detection of prostate-specific antigen

Jiajie Liang [a,1], Cuize Yao [a,1], Xiuqing Li [a], Ze Wu [a], Caihong Huang [a], Qiangqiang Fu [a], Caifeng Lan [a], Donglin Cao [b], Yong Tang [a,*]

[a] Department of Bioengineering, Guangdong Province Key Laboratory of Molecular Immunology and Antibody Engineering, Jinan University, Guangzhou 510632, PR China
[b] Department of Laboratory Medicine, Guangdong No. 2 Provincial People's Hospital, Guangzhou 510317, PR China

ARTICLE INFO

Article history:
Received 5 December 2014
Received in revised form
7 February 2015
Accepted 16 February 2015
Available online 17 February 2015

Keywords:
Plasmonic biosensor
Silver nanoprism
Enzyme-linked immunosorbent assay
Etching
Signal amplification

ABSTRACT

Ultrasensitive and quantitative detection using simple and low-cost assays is critical in clinical diagnostics. In this report, we developed a triangular silver nanoprism (AgNPRs) etching-based plasmonic biosensor for the detection of cancer biomarkers. The triangular AgNPRs-based plasmonic biosensor is an enzyme-linked immunosorbent assay combined with the enzyme-mediated surface plasmon resonance (SPR) of triangular AgNPRs. Triangular AgNPRs uses the immune response of prostate-specific antigen (PSA) to trigger the glucose oxidase (GOx)-catalysed oxidation of glucose (Glu), producing hydrogen peroxide. Hydrogen peroxide acts as an oxidant to etch the triangular AgNPRs into smaller spherical silver nanoparticles, which is accompanied by a substantial blueshift of the SPR peak and a colourimetric blue-to-purple change that can be observed by the naked eye. The SPR peak shift enables the quantitative assessment of PSA due to the remarkable colour change. The triangular AgNPRs-based plasmonic ELISA approach exhibited a quasilinear response to logarithmic PSA concentrations in the range of 10 fg/mL to 100 pg/mL with a limit of detection (LOD) of 4.1 fg/mL. In addition, the LOD of PSA in this approach exceeds that of the conventional HRP-based ELISA (1.25 ng/mL) approach by more than 5 orders of magnitude. Patient serum samples from 16 donors were assayed with triangular AgNPRs-based plasmonic ELISA. The results from the triangular AgNPRs-based immunoassay and the time-resolved fluorescence immunoassay showed excellent correlation, and there were no significant differences in the quantified amounts of PSA. The triangular AgNPRs-based plasmonic ELISA approach has advantages (ultrasensitive, cost-effective, ease of operation) that are expected to be of great interest in diagnostics and to be suitable for a point-of-care test.

1. Introduction

Lowering the limit of detection is the key to the ultrasensitive quantification of clinical biomarkers in complex samples and facilitates early-stage diagnosis, monitoring disease progression, and evaluating therapeutic interventions (Espinoza-Castañeda et al., in press; Giljohann and Mirkin, 2009; Rissin et al., 2010). Currently, the enzyme-linked immunosorbent assay (ELISA) is the most popular immunoassay in clinical biomarker detection and measures protein biomarkers at concentrations above 0.1 ng/mL (Thaxton et al., 2009; Vashist et al., In press). However, the sensitivity of a typical ELISA cannot accommodate the clinical threshold of many biomarkers, which have concentrations in the range of fg/mL to pg/mL in the early stages of a disease (Liu et al., 2013a; Park et al., 2009). Thus, the design of rapid, inexpensive and ultrasensitive sensors for the diagnosis of diseases is extremely important, especially in some resource-constrained countries (Patton et al., 2008; Tang and Hewlett, 2010).

To address this problem, a variety of enhanced immunoassays with ultrahigh sensitivity were developed by usimL noble metal (e.g., Au and Ag) nanomaterial (de La Rica and Stevens, 2012; Rosman et al., 2013; TamL et al., 2013). A noble metal nanomaterial possesses a strong surface plasmon resonance (SPR) absorption and offers unparalleled functionalities when constructing biosensors for highly sensitive detection (He et al., 2012; Hess et al., 2012; Neely et al., 2009; Rodríguez-Lorenzo et al., 2012; Sonntag et al., 2014; Wang et al., 2013). The SPR responses of noble metal nanomaterials are extremely sensitive to structural parameters

* Corresponding autho: Fax: +86 20 85227003.
E-mail address: tyjaq7926@163.com (Y. Tang).
[1] These authors contributed equally to this work.

http://dx.doi.org/10.1016/j.bios.2015.02.026
0956-5663/

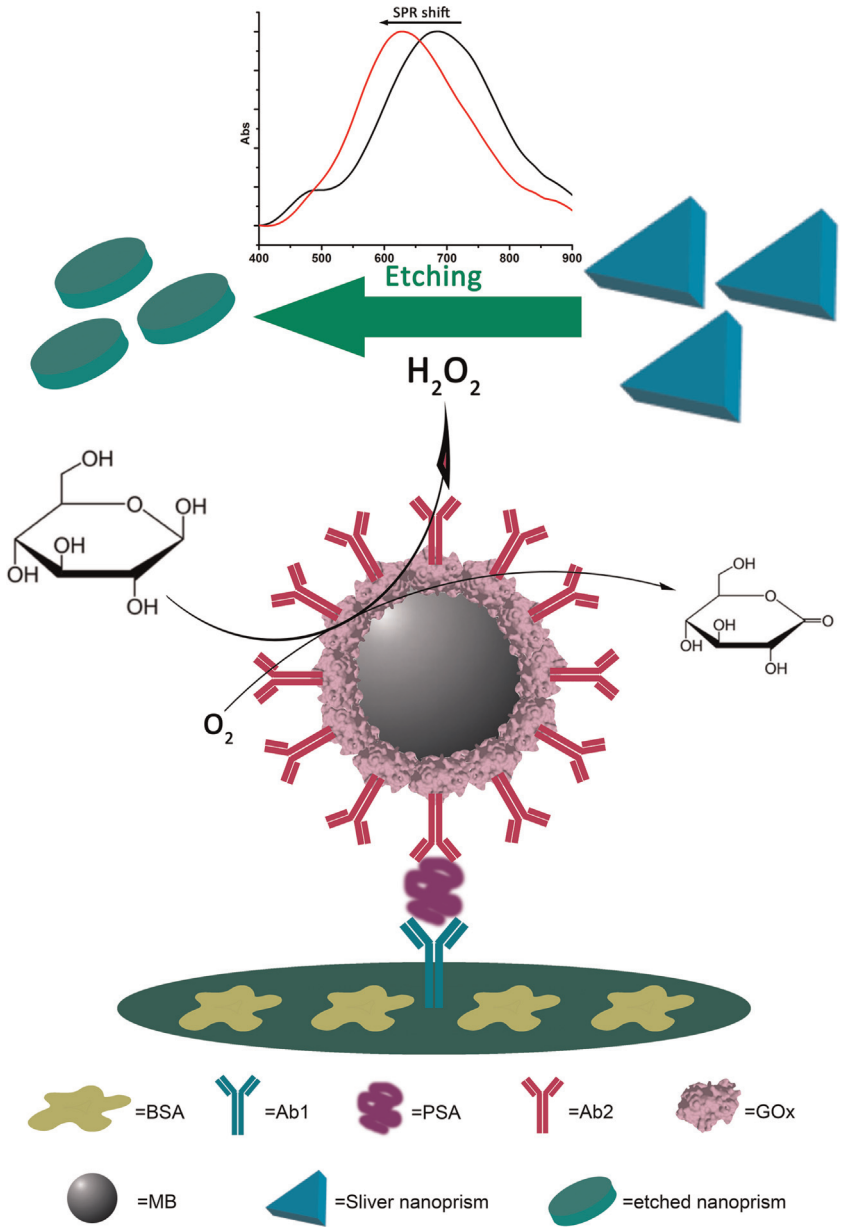

Fig. 1. Schematic diagram of the quantitative immunoassay based on glucose oxidase (GOx)-catalysed etching of triangular silver nanoprisms (AgNPRs) into smaller spherical silver nanoparticles. Prostate-specific antigen (PSA) is first immobilised by the capture antibody (Ab_1), and then PSA is recognised by the detection antibody (Ab_2) conjugated with GOx on the surfaces of the magnetic beads (MBs). The immobilised GOx catalyses the oxidation of glucose (Glu) to generate hydrogen peroxide, which induces the etching of triangular AgNPRs into smaller spherical silver nanoparticles. With the etching, the solution turns blue to purple.

such as size, shape, composition, distance, and the surrounding media, making them the basis for various colorimetric sensors (Elghanian et al., 1997; Howes et al., 2014; Jain et al., 2008; Liu et al., 2013b; Saa et al., 2014; Xie et al., 2012). To date, the aggregation/deaggregation modulation of AuNP-based colorimetric sensing has been well studied in immunoreactions to detect biomarkers and has aroused considerable interest owing to their ultrahigh sensitivity and convenient readout (Jornet-Martinez et al., 2014; Liu et al., 2014; Nie et al., 2014). However, the suspension of the aggregates is unstable and tends to precipitate, leading to colour diminishment because of increased particle size and reduced surface repelling force. Furthermore, most of the reported AuNP-based immunoassays are unable to quantify biomarkers due to their narrow linear detection ranges (de la Rica and Stevens, 2013). It remains a challenge to create ultrasensitive and quantitative immunoassays using other methods and nanomaterials.

Recently, anisotropic noble metal nanomaterials, such as gold nanorods, nanocubes, nanocages, nanostars and nanoflowers, have attracted considerable attention for applications ranging from controllable synthesis to application exploration (Dondapati et al., 2010; Fang et al., 2010; Huang and Lin, 2012; Jakab et al., 2011; Liu et al., 2013c; Skrabalak et al., 2007; Verma et al., 2014). Among these nanomaterials, the silver-based anisotropic nanomaterials have attracted intensive attention due to their strong shape-dependant optical properties (Wiley et al., 2005). Compared to gold nanomaterials, silver anisotropic nanomaterials are promising for the design of wavelength-variation sensing platforms, because silver anisotropic nanomaterials produce a much stronger and sharper plasmon resonance (Gao et al., 2012; Millstone et al., 2009). This method of sensing can potentially overcome the above problems, because signal generation is dependant on particle morphology change instead of the modulation of aggregation/

deaggregation. In particular, we note that triangular nanoprisms contain three sharp vertices or "tips" that contribute significantly to their optical and electronic properties. Technically, triangular AgNPRs with three-dimensional nanostructures exhibit fascinating features in the localised SPR (LSPR) owing to an extreme degree of anisotropy in their structures (Chen et al., 2012; Zhang et al., 2011). It is also well known that triangular AgNPRs can be easily etched into round nanodiscs using hydrogen peroxide, causing a concomitant blueshift of the SPR spectra depending on the change to the particle architecture (Tan et al., 2014; Xia et al., 2013; Yang et al., 2014). This phenomenon has been introduced into a quantitative immunoassay to build a colorimetric sensor that allows the detection of biomarkers in clinical samples. Accordingly, in this study, we demonstrated that plasmonic triangular AgNPRs are applicable to the ultrasensitive measurements of a cancer biomarker in serum (prostate-specific antigen, PSA) in a simple method with few technical demands. The detection limit of the proposed method was 4.1 fg/mL, which was lower than the LOD of the horseradish peroxidase (HRP)-based ELISA and some of nanotechnology-based biosensors (Table S1). Furthermore, these clear blue-to-purple results can be easily distinguished by the naked eye, making the method simple, cost-effective and suitable for point-of-care (POC) diagnostics.

Fig. 1 schematically depicts the working principle of the assay, which combines improved heterogeneous sandwich-type ELISA methods and the inherent sensitivity of plasmonic AgNPRs. The detection sensitivity is expected to be considerably enhanced due to two rounds of amplification. In the first round, detection antibodies (denoted as Ab_2) were conjugated with glucose oxidase (GOx), which catalyses its substrate Glu to generate gluconic acid and hydrogen peroxide. In turn, the hydrogen peroxide acts as an oxidant to etch the triangular AgNPRs into smaller spherical silver nanoparticles, which is accompanied by a substantial blueshift of the SPR peak and a colorimetric blue-to-purple that can be observed by the naked eye. In the second round, magnetic beads (MBs) were used to load many thousands of GOx (76000 GOx per MB in this study) and Ab_2 (Liu et al., 2014). This Ab_2–GOx–MB format can specifically recognise the analyte that was bound by the capture antibody (denoted as Ab_1). The amount of GOx is proportional to the concentration of the detection targets sandwiched by immunoreaction. Very small amounts of the analytes can be detected because of the high density of GOx on MB. Impressively, the proposed sensing method was very convenient: the operation and time for ultra-sensitive detection is similar to that of the horseradish peroxidase (HRP)-based ELISA. Therefore, we believe that such a visual, ultrasensitive, and low-cost biosensor has great potential for point-of-care test (POCT).

2. Materials and methods

2.1. Materials and reagents

Silver nitrate ($AgNO_3$, 99.8%) was obtained from Sinoreagent (Shanghai, China). Chloroauric acid ($HAuCl_4$), TMB (3,3′,5,5′-tetramethylbenzidine) and Tween-20 were obtained from Amresco, USA. Horseradish peroxidase (HRP), bovine serum albumin (BSA) and PSA were purchased from Sigma-Aldrich. Trisodium citrate was purchased from Damaoreagent (Tianjin, China). Foetal bovine serum was obtained from Life Technology. N-hydroxysuccinimide-activated MBs (NHS-MBs) with a diameter of approximately 1 μm were purchased from Fisher Scientific. DBCO-PEG_4-NHS ester (NHS-DBCO) and Azido-PEG4-NHS ester (NHS-azide) were purchased from Click Chemistry Tools. The 96-well polystyrene plate was purchased from JET BIOFIL. The monoclonal primary antihuman PSA antibody (PSA-Ab_1) and secondary antihuman PSA antibody (PSA-Ab_2) were obtained from UcallM. The serum samples were collected from the Department of Laboratory Medicine, Guangdong No. 2 Provincial People's Hospital. The hydrogen peroxide (H_2O_2, 30 wt%), $NaBH_4$, H_2SO_4 and potassium carbonate were purchased from GZ chemical reagent (Guangzhou, China). Deionised water (Milli-Q grade, Millipore) with a resistivity of 18.2 MΩ cm was used throughout this study.

2.2. Apparatus

The SPR spectrums of triangular AgNPRs solutions in 96-well plates were collected by a Synergy H1 Hybrid Multi-Mode Microplate Reader (Bio-Tek Instruments, Inc.). The absorbance of the HRP-based ELISA was measured at 450 nm using a MK3 microplate reader. Characterisations using transmission electron microscopy (TEM) were performed with a PHILIPS TECNAI-10 transmission electron microscope operating at an acceleration voltage of 120 kV. The samples for TEM measurements were prepared by the deposition of one drop of aqueous dispersion onto a copper grid coated with thin films of carbon, and the solvent was removed by evaporation in air.

2.3 Identification of the triangular AgNPRs-based assay

The triangular AgNPRs were synthesised according to a reported procedure (Zhang et al., 2011). Details of procedure are available as Supplementary information. H_2O_2 was first diluted with deionised water to various concentrations ranging from 0 μM to 90 μM. The triangular AgNPRs solution was added to each of the concentrations of H_2O_2. The mixtures were incubated at room temperature for 30 min. A photograph was taken, and the corresponding SPR spectrum was collected.

GOx solutions at various concentrations ranging from 0 to 1 μg/mL were incubated with Glu (0.5 mM) in water at 37 °C for 30 min, and the triangular nanoprism solutions was added to the resulting solutions. The mixtures were then incubated at room temperature for 40 min. A photograph was taken, and the corresponding SPR spectrum was collected.

2.4 Procedure of silver triangular nanoprism-based immunoassay for PSA detection

Before the immunoassay, Ab_2–GOx–MBs were first prepared. Details of preparation are available as Supplementary information. In this modified ELISA method, 96-well polystyrene plates were modified with Ab_1 diluted in PBS at 4 °C overnight. After washing the plates three times with wash buffer (1% Tween-20 in PBS), the plates were blocked with blocking buffer (1 mg/mL BSA in PBS) at 37 °C for 1 h. Subsequently, the plates were washed three times with wash buffer, and PSA was added to the desired final concentration by diluting foetal bovine serum. After 1 h, the plates were washed three times with wash buffer, and 0.1 mg/mL Ab_2–GOx–MBs was added at 37 °C for 1 h. Then, three washing steps were performed using Glu (1 mm) in 50 μL of water at 37 °C for 30 min. Then, the supernatant was mixed with the silver triangular nanoprisms for 40 min. A photograph was taken, and the corresponding SPR spectrum was collected. The HRP-based ELISA was compared with AgNPRs-based immunoassay. The procedure of HRP-based ELISA is available as Supplementary information.

3. Results and discussion

3.1 Hydrogen peroxide etching

It is well known that hydrogen peroxide is a powerful oxidising

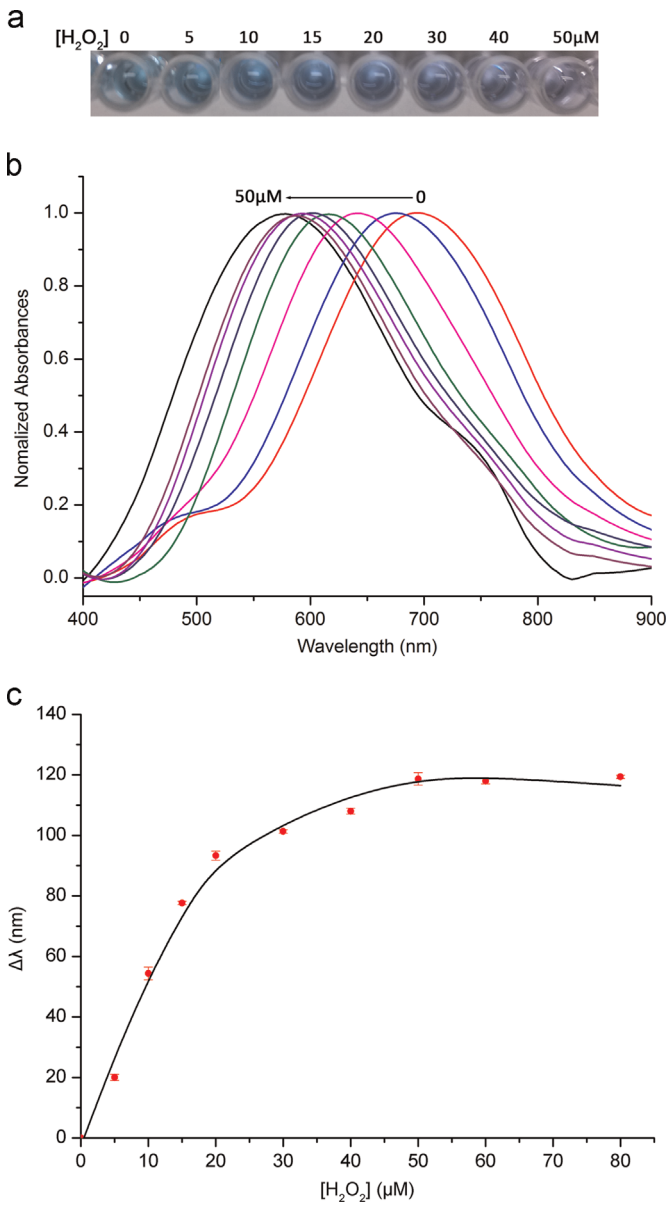

Fig. 2. Verification of the etching of triangular AgNPRs in the presence of hydrogen peroxide. (a) With the addition of varying concentrations of hydrogen peroxide into the triangular AgNPR solutions, the solutions changed gradually. (b) SPR peaks of the triangular AgNPRs in the presence of different concentrations of hydrogen peroxide. (c) Peak shift values were plotted against various concentrations of hydrogen peroxide. Each value represents the mean of three independent experiments ($n=3$).

agent with a strong dependence on the acidity of the solution (Ho et al., 2010). Under acidic conditions,

$H_2O_2+2H^++2e^-\rightarrow 2H_2O$ $E^0=1.763$ V.

Under alkaline conditions,

$H_2O_2+2e^-\rightarrow 2OH^-$ $E^0=0.867$ V.

However, for the AgNPs, their redox potential is determined as follows:

$Ag^++e^-\rightarrow Ag$ $E^0=0.7996$ V.

AgNPs have a standard potential of 1.763 V in acidic solutions and 0.867 V in alkaline solutions, both of which are higher than Ag^+/Ag (0.7996 V), suggesting that hydrogen peroxide can be used as an effective oxidising agent to dissolve metallic silver. To

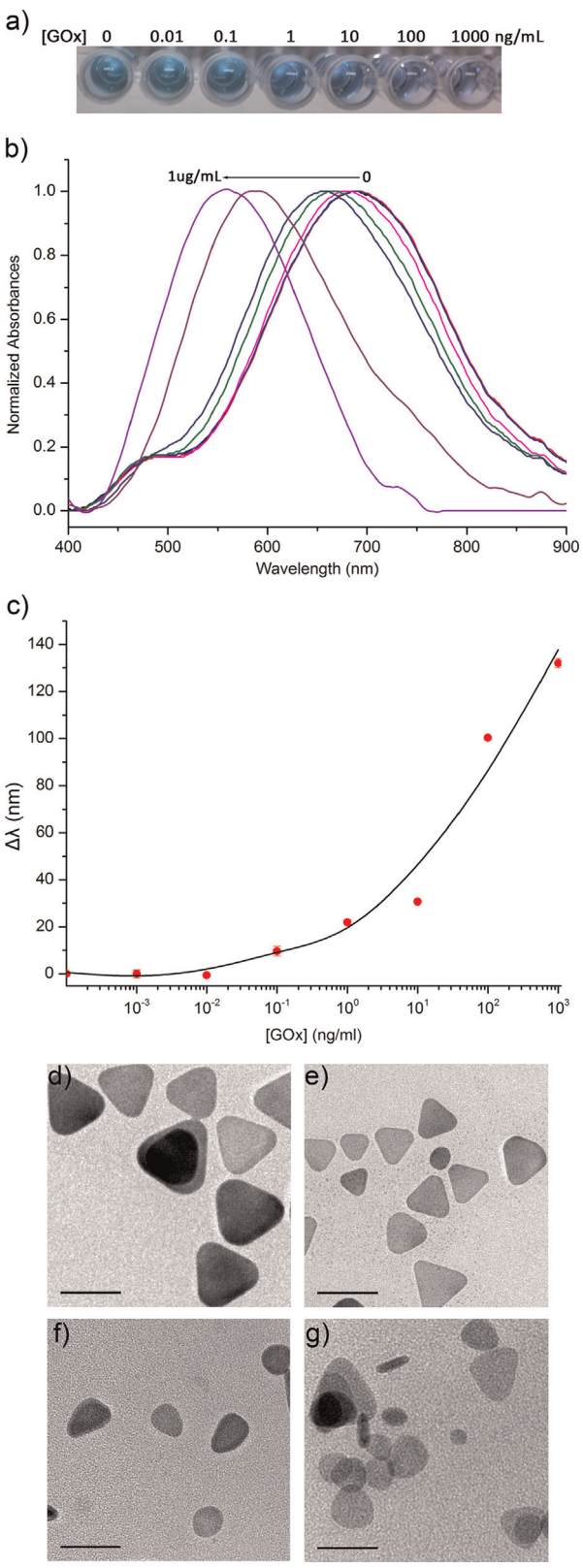

Fig. 3. Verification of the etching of triangular AgNPRs in the presence of GOx. (a) With the addition of varying concentrations of GOx to the triangular AgNPRs solutions containing Glu, the solutions changed gradually. (b) SPR peaks of triangular AgNPRs in the presence of different concentrations of GOx. (c) Peak shift values were plotted against various concentrations of GOx. Each value represents the mean of three independent experiments ($n=3$). (d) TEM images of triangular AgNPRs and (e–g) the shape change during the etching process (scale bar is 50 nm). Reaction time corresponding to TEM images e–g is 10 min, 20 min and 30 min, respectively. Aspect ratio corresponding to TEM images d–g is 10, 9, 6 and 4, respectively.

demonstrate this concept and to investigate the impact of hydrogen peroxide on the etching of triangular AgNPRs, different concentrations of hydrogen peroxide were added to the triangular AgNPRs solutions, and the solutions were inspected using UV–vis spectrometry. The resulting solutions were incubated at room temperature for 30 min (see the dynamic process in Fig. S1). As shown in Fig. 2a and b, as the concentration of hydrogen peroxide increases, the solutions gradually turn purple and the SPR peak shows a gradual blueshift. The shift intensity and the colour change are highly associated with the concentration of hydrogen peroxide. By collecting the wavelengths of the SPR peaks for each solution, we found that the intensity of the blueshift is linear between 0 and 20 μM (Fig. 2c), suggesting the feasibility of this strategy to quantify the target molecule concentration.

3.2 Glu oxidase-catalysed oxidation

On the basis of the literature and the above experiments, we therefore concluded that the SPR blueshift of the triangular AgNPRs was caused by the etching effect of hydrogen peroxide. Next, we studied the impact of GOx on the etching of triangular AgNPRs according to the following reactions (Zhang et al., 2010):

$$\text{Glucose} + O_2 \rightarrow \text{gluconic acid} + H_2O_2$$

$$\text{Metallic Ag} + H_2O_2 \rightarrow Ag^+ + H_2O$$

Additionally, the GOx-catalysed oxidation of Glu produces gluconic acid, which effectively lowers the local pH and consequently increases the oxidising power to accelerate the etching process. Fig. S2 shows the optimal pH values on the Glu oxidase-catalysed oxidation is 7, and we finished the following experiment under the pH=7. First, we tested the influence of Glu, GOx, Ab_1, Ab_2 and PSA on the stability of the triangular AgNPRs. No SPR peak shifts were observed upon the addition of these constituents (Fig. S3), demonstrating the feasibility of using triangular AgNPRs as the indicator in our assay. Next, to optimise the enzymatic reaction, we studied the time-dependant evolution of the SPR spectra in the triangular AgNPRs–Glu system incubated with GOx. GOx was first mixed with Glu at 37 °C to produce various amounts of hydrogen peroxide, and then the triangular AgNPRs were added to the resulting solutions. Fig. S4 shows the time-dependant SPR spectra of the homogeneous system incubated with GOx. It was observed that the blueshift intensity gradually decreases and levels off to a saturation value after approximately 35 min. Subsequently, we determined the SPR peak of the triangular AgNPRs in the presence of different concentrations of GOx. As shown in Fig. 3a and b, the gradual blueshift of the SPR peak and the distinct colour change of the triangular AgNPRs (blue→purple) were observed as the concentration of GOx increases. Higher GOx concentrations produced larger blueshifts of the SPR peak, which is useful for the development of a highly sensitive immunoassay (Fig. 3c). It was observed that the etching process is GOx-concentration dependant. TEM images indicated that the morphology of the triangular silver nanoprisms gradually changed from triangular to spherical (Fig. 3d–g). Finally, we compared the sensitivity of AgNPRs with different aspect ratios and silver nanoparticles (Fig. S5a and b). The results showed that with a decrease in aspect ratio, the sensitivity decreased. Meanwhile, the silver nanoparticles were not suitable for the development of sensitive assays using the SPR shift as an analytical signal (Fig. S5c).

3.3 Triangular silver nanoprism etching-based immunoassay for PSA detection

After demonstrating that hydrogen peroxide can etch triangular AgNPRs and also causes the SPR peak blueshift, we

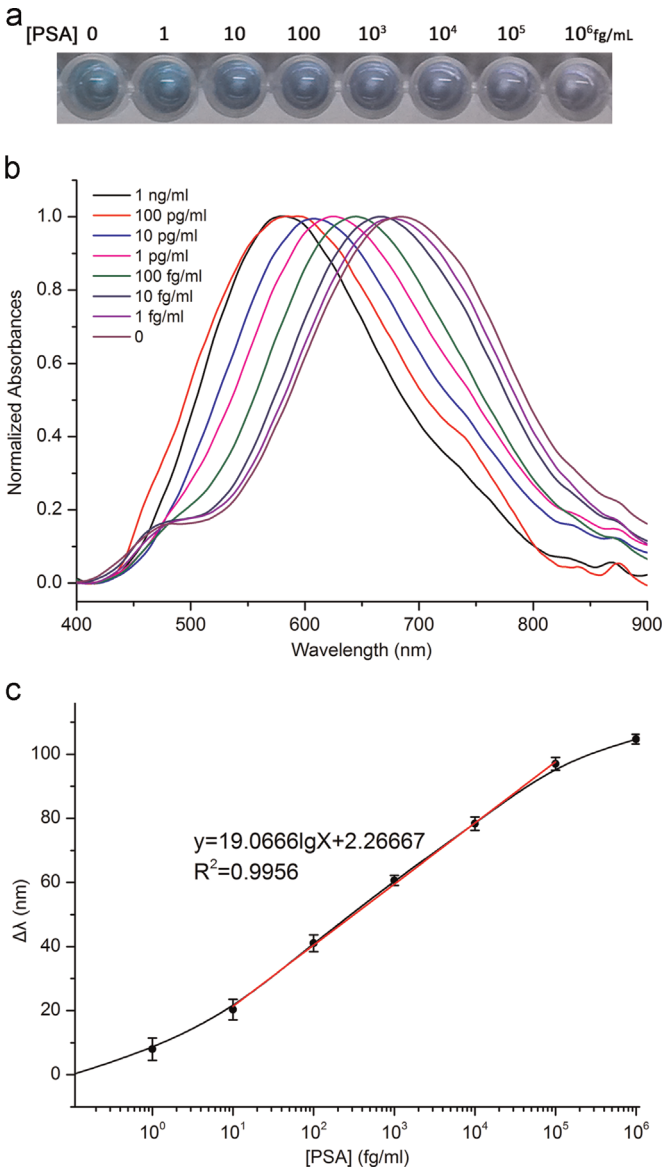

Fig. 4. Quantitative immunoassay of PSA in sera samples. (a) Naked-eye detection of PSA with different concentrations in foetal bovine sera. (b) SPR peak shifts of triangular AgNPRs with different concentrations of PSA in foetal bovine sera. (c) Peak shifts of triangular nanoprisms compared to the concentration of PSA. Each value represents the mean of three independent experiments (n=3).

attempted to bring this approach to the immunoassays. We first prepared the Ab_2 and GOx co-modified MBs (Ab_2–GOx–MBs) using a step-by-step procedure. Inorganic biological hybrid nanomaterial, such as gold nanoparticle (AuNP) (Ambrosi et al., 2010; Li et al., 2014), graphene (Lin et al., 2013; Xu et al., 2013), carbon-nanotube (Wang et al., 2004) and MBs (Munge et al., 2011), can be massively co-modified by antibodies and enzymes, especially MBs, which was reported to be an excellent carrier that can load many thousands of enzymes for signal amplification and also maintain activity (Liu et al., 2013b; Munge et al., 2011). In this study, we chose N-hydroxysuccinimide (NHS)-activated MB to load GOx (approximately 76000 GOx per MB), and the resulting GOx-coated beads were conjugated with Ab_2 via copper-free click chemistry. Fig. S6 shows the UV–vis spectrum of MBs, GOx–MBs and Ab_2–GOx–MBs. There are some absorption peaks in the ultraviolet range, which may be the distinct absorption peaks of the –NHS on MBs. Absorption peaks around 275 nm and 280 nm severally appear in the

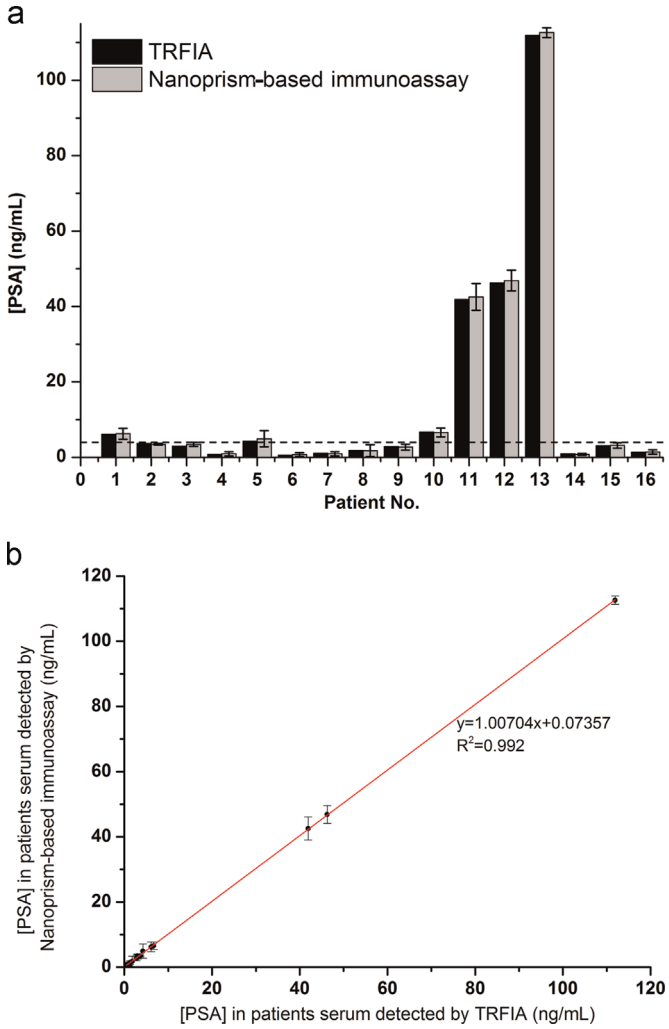

Fig. 5. (a) Results of the quantitative detection of PSA in clinical samples by the triangular AgNPRs-based immunoassay compared with TRFIA. (b) The correlation analysis between the triangular AgNPRs-based immunoassay and TRFIA. Each value represents the mean of three independent experiments ($n=3$).

GOx–MBs spectrum and Ab_2–GOx–MBs spectrum, which confirms a successful attachment of GOx and Ab_2 onto the MBs surfaces. After synthesis of the Ab_2–GOx–MBs, we applied the triangular AgNPRs–Glu system to test the GOx-like activity that catalyses the oxidation of Glu to generate hydrogen peroxide. The SPR peaks of triangular AgNPRs were assessed in the presence of different concentrations of Ab_2–GOx–MBs. We observed that the solutions turned purple gradually, and the blueshift of the SPR peak is highly related to the concentration of Ab_2–GOx–MBs, which was further confirmed by the change of the SPR peak wavelength. As shown in Fig. S7, as the concentration of Ab_2–GOx–MBs increases, the SPR peak gradually blueshifts and the SPR peak wavelength changes over a wide linear range when there are more than 10^4 particles /mL.

Then, the triangular AgNPRs–Glu system was subsequently adapted for use with the sandwich ELISA for PSA detection, which is a classical prostate cancer biomarker approved by the Food and Drug Administration (FDA). Herein, varying concentrations of PSA (1–10^6 fg/mL) were added to foetal bovine sera. The foetal bovine sera-only samples were set as the blanks. In this case, the colour of the triangular AgNPRs solutions changed from blue to purple, which can be easily differentiated by the naked eye (Fig. 4a). The lowest detectable concentration of PSA in which the purple colour can be clearly discriminated by the naked eye was 10 fg/mL. Furthermore, we measured the target concentration-dependant SPR peak shift process. As shown in Fig. 4b, the SPR peak shifted when the concentration of PSA was between 1 fg/mL and 10^6 fg/mL, demonstrating that the etching of the AgNPRs by hydrogen peroxide is strongly dependant on the concentration of PSA. The linear detection range is from 10 to 10^5 fg/mL (Fig. 4c). This linear range is wide, suggesting that our immunoassay has great promise for the quantitative detection of biomarkers with concentrations ranging from fg/mL to pg/mL. The LOD defined by a signal-to-noise ratio of 3 was determined to be 4.1 fg/mL. The reproducibility expressed in terms of the relative standard deviation (RSD) was about 2.5% ($n=3$) at a PSA concentration of 10^3 fg/mL, indicating a good reproducibility of the proposed immunoassay. The HRP-based ELISA, the most commonly used approach for clinical biomarker detection, was compared with our colourimetric assay. The lowest detectable concentration of PSA using an HRP-based ELISA with the same antibodies was 1.25 ng/mL (Fig. S8), which was five orders of magnitude higher than the LOD of our system. These results clearly demonstrated the ability of triangular silver nanoprism etching as a general method for immunodetection with ultrasensitivity.

In order to assess the selectivity of the immunoassay, specificity experiment was performed using 1 ng/mL PSA, bovine serum albumin (BSA), horseradish peroxidase (HRP), CK-MB and α-fetoprotein (AFP). The result indicated that there was almost no blueshift of the SPR peaks using BSA, HRP, CK-MB and AFP (Fig. S9), suggesting a high selectivity of the developed immunoassay.

3.4 Detection of clinical samples

Encouraged by the excellent sensitivity and wide linear detection range for PSA detection, the sera from 16 donors were assayed by this system to evaluate the capability of our assay in the real world. These donors were suspected prostate cancer patients whose PSA levels have been previously determined using the time resolved fluorescence immunoassay (TRFIA). To demonstrate that the triangular silver nanoprism-based immunoassay can accurately quantify target molecules in biological samples, the suspected patient sera samples were diluted 1000-fold in foetal bovine serum to correspond to the linear range of the calibration curve. The differentiation of positive and negative signals depended on the clinical threshold, which is indicated by the horizontal dotted line (Fig. 5a). Moreover, the correlation analysis between nanoprism-based immunoassay and TRFIA was shown (Fig. 5b). The results from two method showed excellent correlation, and no significant differences in the quantified amounts of PSA were observed ($P>0.05$). These results indicate that the triangular silver nanoprism-based immunoassay can be used for the identification of very low concentrations of cancer protein biomarkers in clinical samples. Owing to high method sensitivity, the clinical samples can be repeatedly diluted, thus reducing the interference from other substances. Because of the simplicity and efficacy of this method, the proposed biosensor has great potential for POC diagnostic applications, especially for rural populations in third world countries.

4. Conclusions

By taking advantage of the unique optical properties of triangular AgNPRs and the etching effect of hydrogen peroxide generated from the enzymatic oxidation of Glu, we successfully developed a simple sensor for detecting cancer biomarkers in clinical samples using the triangular AgNPRs–GOx signal system. Unlike traditional plasmonic sensors, which generally depend on the modulation of aggregation/deaggregation of noble metal

nanoparticles, this assay is based on an etching process, in which the shape and size of the nanoprisms are altered and accompanied by an SPR shift. Although the poor chemical and structural stability of the triangular AgNPRs are the main issue that prevents their broad use, recent reports have indicated that anisotropic nanoprisms possess well-defined, facet-dependant physicochemical properties. It is therefore essential to develop strategies in which analyte targets can be colourimetrically visualised by shape-dependant SPR peak shifts, because colourimetry is useful for both basic research and clinical applications. This method combined enzymes and MBs with ELISA, which greatly lowered the detection limit. The results indicated that this plasmonic biosensor can detect biomarkers at concentrations as low as 4.1 fg/mL by simple mixing and in a wide linear range from fg/mL to pg/mL. Moreover, this biosensor was also more convenient than conventional HRP-based ELISA, which makes it a promising platform for biomedical applications. In addition, the sensor does not require a sophisticated experimental procedure or equipment. Considering the ultrahigh sensitivity and versatility of this plasmonic assay, it has potential application in point-of-care diagnostics. Although only PSA was detected in this study, the approach reported here is generalisable and can be easily applied to other ELISA systems.

Acknowledgements

This work was supported by the Technology Research Program of Guangdong Province (2013B010404027) and Technology Research Program of Guangzhou City (2014J4100010). This manuscript has been edited and proofread by NPG Language Editing.

Appendix A. Supplementary Information

Supplementary data associated with this article can be found in the online version at http://dx.doi.org/10.1016/j.bios.2015.02.026.

References

Ambrosi, A., Airo, F., Merkoci, A., 2010. Anal. Chem. 82 (3), 1151–1156.
Chen, L., Fu, X., Lu, W., Chen, L., 2012. ACS Appl. Mater. Interfaces 5 (2), 284–290.
de La Rica, R., Stevens, M.M., 2012. Nat. Nanotechnol. 7 (12), 821–824.
de la Rica, R., Stevens, M.M., 2013. Nat. Protoc. 8 (9), 1759–1764.
Dondapati, S.K., Sau, T.K., Hrelescu, C., Klar, T.A., Stefani, F.D., Feldmann, J., 2010. ACS Nano 4 (11), 6318–6322.
Elghanian, R., Storhoff, J.J., Mucic, R.C., Letsinger, R.L., Mirkin, C.A., 1997. Science 277 (5329), 1078–1081.
Espinoza-Castañeda, M., Escosura-Muñiz, A.D.L., Chamorro, A., Torres, C.D., Merkoçi, A., 2015. Biosens. Bioelectron, in press.
Fang, J., Du, S., Lebedkin, S., Li, Z., Kruk, R., Kappes, M., Hahn, H., 2010. Nano Lett. 10 (12), 5006–5013.
Gao, C., Lu, Z., Liu, Y., Zhang, Q., Chi, M., Cheng, Q., Yin, Y., 2012. Angew. Chem. Int. Ed. 51 (23), 5629–5633.
Giljohann, D.A., Mirkin, C.A., 2009. Nature 462 (7272), 461–464.
He, H., Xu, X., Wu, H., Jin, Y., 2012. Adv. Mater. 24 (13), 1736–1740.
Hess, O., Pendry, J., Maier, S., Oulton, R., Hamm, J., Tsakmakidis, K., 2012. Nat. Mater. 11 (7), 573–584.
Ho, C.-M., Yau, S.K.-W., Lok, C.-N., So, M.-H., Che, C.-M., 2010. Chem. Asian J. 5 (2), 285.
Howes, P.D., Rana, S., Stevens, M.M., 2014. Chem. Soc. Rev. 43 (11), 3835–3853.
Huang, M.H., Lin, P.H., 2012. Adv. Funct. Mater. 22 (1), 14–24.
Jain, P.K., Huang, X., El-Sayed, I.H., El-Sayed, M.A., 2008. Acc. Chem. Res. 41 (12), 1578–1586.
Jakab, A., Rosman, C., Khalavka, Y., Becker, J., Trügler, A., Hohenester, U., Sönnichsen, C., 2011. ACS Nano 5 (9), 6880–6885.
Jornet-Martinez, N., González-Béjar, M., Moliner-Martínez, Y., Campíns-Falcó, P., Pérez-Prieto, J., 2014. Anal. Chem. 86 (3), 1347–1351.
Li, Y., Zhou, Y., Meng, X., Zhang, Y., Liu, J., Zhang, Y., Wang, N., Hu, P., Lu, S., Ren, H., 2014. Biosens. Bioelectron. 61, 241–244.
Lin, H., Liu, Y., Huo, J., Zhang, A., Pan, Y., Bai, H., Jiao, Z., Fang, T., Wang, X., Cai, Y., Wang, Q., Zhang, Y., Qian, X., 2013. Anal. Chem. 85 (13), 6228–6232.
Liu, D., Huang, X., Wang, Z., Jin, A., Sun, X., Zhu, L., Wang, F., Ma, Y., Niu, G., Hight Walker, A.R., 2013a. ACS Nano 7 (6), 5568–5576.
Liu, D., Wang, Z., Jin, A., Huang, X., Sun, X., Wang, F., Yan, Q., Ge, S., Xia, N., Niu, G., 2013b. Angew. Chem. Int. Ed. 52 (52), 14065–14069.
Liu, D., Yang, J., Wang, H.-F., Wang, Z., Huang, X., Wang, Z., Niu, G., Hight Walker, A. R., Chen, X., 2014. Anal. Chem. 86 (12), 5800–5806.
Liu, X., Zhang, S., Tan, P., Zhou, J., Huang, Y., Nie, Z., Yao, S., 2013c. Chem. Commun. 49 (18), 1856–1858.
Millstone, J.E., Hurst, S.J., Métraux, G.S., Cutler, J.I., Mirkin, C.A., 2009. Small 5 (6), 646–664.
Munge, B.S., Coffey, A.L., Doucette, J.M., Somba, B.K., Malhotra, R., Patel, V., Gutkind, J.S., Rusling, J.F., 2011. Angew. Chem. 123 (34), 8061–8064.
Neely, A., Perry, C., Varisli, B., Singh, A.K., Arbneshi, T., Senapati, D., Kalluri, J.R., Ray, P.C., 2009. ACS Nano 3 (9), 2834–2840.
Nie, X.-M., Huang, R., Dong, C.-X., Tang, L.-J., Gui, R., Jiang, J.-H., 2014. Biosens. Bioelectron. 58, 314–319.
Park, J.-S., Cho, M.K., Lee, E.J., Ahn, K.-Y., Lee, K.E., Jung, J.H., Cho, Y., Han, S.-S., Kim, Y. K., Lee, J., 2009. Nat. Nanotechnol. 4 (4), 259–264.
Patton, J.C., Coovadia, A.H., Meyers, T.M., Sherman, G.G., 2008. Clin. Vaccine Immunol. 15 (2), 388–391.
Rissin, D.M., Kan, C.W., Campbell, T.G., Howes, S.C., Fournier, D.R., Song, L., Piech, T., Patel, P.P., Chang, L., Rivnak, A.J., 2010. Nat. Biotechnol. 28 (6), 595–599.
Rodríguez-Lorenzo, L., de La Rica, R., Álvarez-Puebla, R.A., Liz-Marzán, L.M., Stevens, M.M., 2012. Nat. Mater. 11 (7), 604–607.
Rosman, C., Prasad, J., Neiser, A., Henkel, A., Edgar, J., Sönnichsen, C., 2013. Nano Lett. 13 (7), 3243–3247.
Saa, L., Coronado-Puchau, M., Pavlov, V., Liz-Marzán, L.M., 2014. Nanoscale 13 (6), 7405–7409.
Skrabalak, S.E., Au, L., Li, X., Xia, Y., 2007. Nat. Protoc. 2 (9), 2182–2190.
Sonntag, M.D., Klingsporn, J.M., Zrimsek, A.B., Sharma, B., Ruvuna, L.K., Van Duyne, R.P., 2014. Chem. Soc. Rev. 43 (4), 1230–1247.
Tan, K., Yang, G., Chen, H., Shen, P., Huang, Y., Xia, Y., 2014. Biosens. Bioelectron. 59, 227–232.
Tang, L., Casas, J., Venkataramasubramani, M., 2013. Anal. Chem. 85 (3), 1431–1439.
Tang, S., Hewlett, I., 2010. J. Infect. Dis. 201 (Supplement 1), S59–S64.
Thaxton, C.S., Elghanian, R., Thomas, A.D., Stoeva, S.I., Lee, J.-S., Smith, N.D., Schaeffer, A.J., Klocker, H., Horninger, W., Bartsch, G., 2009. Proc. Natl. Acad. Sci. USA 106 (44), 18437–18442.
Vashist, S.K., Marion Schneider, E., Luong, J.H., 2015. Biosens. Bioelectron. (In press).
Verma, M.S., Chen, P.Z., Jones, L., Gu, F.X., 2014. RSC Adv. 4 (21), 10660–10668.
Wang, F., Liu, X., Lu, C.-H., Willner, I., 2013. ACS Nano 7 (8), 7278–7286.
Wang, J., Liu, G.D., Jan, M.R., 2004. J. Am. Chem. Soc. 126 (10), 3010–3011.
Wiley, B., Sun, Y., Mayers, B., Xia, Y., 2005. Chemistry—Eur. J. 11 (2), 454–463.
Xia, Y., Ye, J., Tan, K., Wang, J., Yang, G., 2013. Anal. Chem. 85 (13), 6241–6247.
Xie, X., Xu, W., Liu, X., 2012. Acc. Chem. Res. 45 (9), 1511–1520.
Xu, H., Wang, D., He, S., Li, J., Feng, B., Ma, P., Xu, P., Gao, S., Zhang, S., Liu, Q., Lu, J., Song, S., Fan, C., 2013. Biosens. Bioelectron. 50, 251–255.
Yang, X., Yu, Y., Gao, Z., 2014. ACS Nano 8 (5), 4902–4907.
Zhang, Q., Cobley, C.M., Zeng, J., Wen, L.-P., Chen, J., Xia, Y., 2010. J. Phys. Chem. C 114 (14), 6396–6400.
Zhang, Q., Li, N., Goebl, J., Lu, Z., Yin, Y., 2011. J. Am. Chem. Soc. 133 (46), 18931–18939.